Composites Communications 47 (2024) 101877

Contents lists available at ScienceDirect

Composites Communications

journal homepage: www.elsevier.com/locate/coco

Short Communication

Ultraweakly low-dispersion epsilon-negative response of GR-CNT/PVDF ternary metacomposites

Jiangnan Yuan [a], Yunlei Zhou [b,**], Farid Manshaii [c], Shaolei Wang [c], Junyi Yin [c], Dongchan Li [a,***], Shizhao Wang [a], Yunpeng Qu [d,*]

[a] School of Chemical Engineering, Hebei University of Technology, Engineering Research Center of Chemical Technology for Efficient Utilization of Seawater Resources, Ministry of Education, 300401, Tianjin, China

[b] Hangzhou Institute of Technology, Xidian University, Hangzhou, 311231, China

[c] Department of Bioengineering, University of California, Los Angeles, Los Angeles, CA, 90095, United States

[d] College of Physics, Guizhou University, Guiyang, 550025, China

ARTICLE INFO

Keywords:
Negative permittivity
Metacomposites
Percolation

ABSTRACT

The epsilon-negative ($\varepsilon' < 0$) response displayed by metacomposites offers notable potential for diverse applications in the design of dielectric and electromagnetic (EM) devices, underpinned by novel principles. However, achieving a weakly low-dispersion ε'-negative performance within the radio frequency (RF) band remains challenging. In this study, we bypassed this issue by constructing three-dimensional (3D) conductive networks through the integration of graphene (GR) and carbon nanotubes (CNT) with polyvinylidene fluoride (PVDF) serving as the matrix material. Leveraging the modifiable GR-CNT network, a ε'-negative response at approximately −20 was attained spanning the 100 MHz-1 GHz range. This ultraweak ε'-negative response was attributed to the formation of a moderate plasmonic state of free carriers within the metacomposites. Further, simulations were conducted, assessing the electric field vector distribution of the ε'-negative materials, revealing promising EM shielding performance. Concurrently, this investigation elucidates the RF ε'-negative response mechanism, paving the way for the practical application of metacomposites.

1. Introduction

Negative permittivity ($\varepsilon' < 0$) has garnered significant attention in recent decades due to its pivotal role in energy storage, antenna configurations and EM shielding [1–3]. Among the various well-designed metacomposites, such as metallic-based, conductive ceramic-embedded, and structural nano-carbon infused percolative composites [3–5], the chemical composition and functional percolative networks are considered critical determinants in modulating negative permittivity [4]. Specifically, the tailoring of the ε'-negative response is based on the comprehensive design strategy for each metacomposite component, correlating with application prerequisites like invisibility, innovative sensors, and high-performance EM shielding [4,5]. Although this flexibility in material design can accommodate intricate operational scenarios of ε'-negative components, such as extreme temperatures, strong corrosion, and strenuous mechanical conditions, formulating universal design principles remains an intricate endeavor [6]. Consequently, extensive research efforts have been channeled toward identifying the optimal material systems with discernible dielectric response mechanisms and corresponding tunable ε'-negative properties [7–11].

Metals, due to their capacity to provide abundant free electrons under an external electrical field, can elicit pronounced negative permittivity behavior in the RF domain, albeit with substantial energy loss [7–9]. Stemming from this observation, some researchers have combined both metal and ceramic constituents to construct adjustable metallic networks. Classic examples include Ni/$BaTiO_3$ [8], Ag/$CaCu_3Ti_4O_{12}$ [9], and Cu/TiO_2 [10], which reduced effective electron concentration and dielectric loss. Apart from metallic composites, carbon nanomaterials, characterized by moderate free carrier concentration and controllable geometric morphology, have emerged as promising candidates for functional fillers in metacomposites. Electrically insulating polymers, substituting ceramic matrices, can curtail the

* Corresponding author.
** Corresponding author.
*** Corresponding author.
E-mail addresses: zhouyunlei@xidian.edu.cn (Y. Zhou), dongchanli@hebut.edu.cn (D. Li), ypqu@gzu.edu.cn (Y. Qu).

https://doi.org/10.1016/j.coco.2024.101877
Received 16 January 2024; Received in revised form 26 February 2024; Accepted 5 March 2024
Available online 6 March 2024

conductive channels within the resultant 3D carbon networks [11,12]. Such an approach offers myriad advantages: enhanced adjustability of the 3D percolative network, effective diminishment of negative permittivity value and dielectric loss, and scalable and facile fabrication of metacomposites [13]. Therefore, carbon/polymer metacomposites could lead to a fine-tunable ε'-negative response with excellent EM shielding performance. This suggests that the perennial challenge of attaining a low-dispersion, a weak ε'-negative response at the RF band might be more feasibly addressed using carbon/polymer metacomposites compared to their metal/ceramic counterparts.

In this context, we fabricated GR-CNTs/PVDF ternary metacomposites, featuring a randomly structured 3D network of 2-dimensional (2D) GR sheets and 1-dimensional (1D) CNT. The mass ratio of GR and CNT is 1:1. The conductive pathway in the GR-CNT framework was modulated by the quasi-spherical PVDF (0-dimensional particles) matrix, tempering the concentration of free carriers. By carefully calibrating the composition, we achieved tunable and weakly negative permittivity values spanning 10^1 to 10^2 orders of magnitude within the metacomposites. This tunability stems from adjustable low-frequency collective plasma oscillations within the 3D carbon network. More importantly, the dispersion characteristic of ε'-negative response was kept consistently around approximately −30 over the 100 MHz-1 GHz domain. Comprehensive simulations further expounded upon the EM shielding potential of these metacomposites, underscoring their viability for next-generation EM device applications.

2. Results and discussion

2.1. Network formation of GR-CNT within metacomposites

Fig. 1a–c demonstrates that the PVDF constituted the major component of the metacomposite. The FESEM and TEM images (Fig. 1g) revealed the presence of micro-sized aggregates dispersed throughout the composite. GR sheets and fiber-like CNT (at 6 wt%, 10 wt%, and 12 wt%) appeared sporadically, surrounded by agglomerated PVDF, indicating a low distribution of the nanofillers within the polymer matrix. However, as the GR-CNT content increased to 14 wt% and 16 wt%, a noticeable exposure of conductive components occurred on the surface and at the interface of the PVDF matrix (as shown in Fig. 1d and e), suggesting a higher degree of dispersion and alignment of the GR-CNT nanofillers. This resulted in a more extensive 3D network structure characterized by multi-directional interweaving, where CNTs served as pillars and GR sheets as structural walls. Additionally, the XRD data (Fig. 1f) confirmed that PVDF comprised a substantial portion of the composite material. Conversely, the conductive material intercalated within the system exhibited negligible characteristic peaks, attributed to the diffraction peaks' diminished intensity from GR-CNT fillers and their lower loading level. This finding accentuates the material's advantages, requiring minimal doping and offering cost-effectiveness. The TG-DSC characterization in Fig. 1h and i illustrates that the obtained composites hold great thermal stability up to ∼400 °C and then start the endothermic reaction.

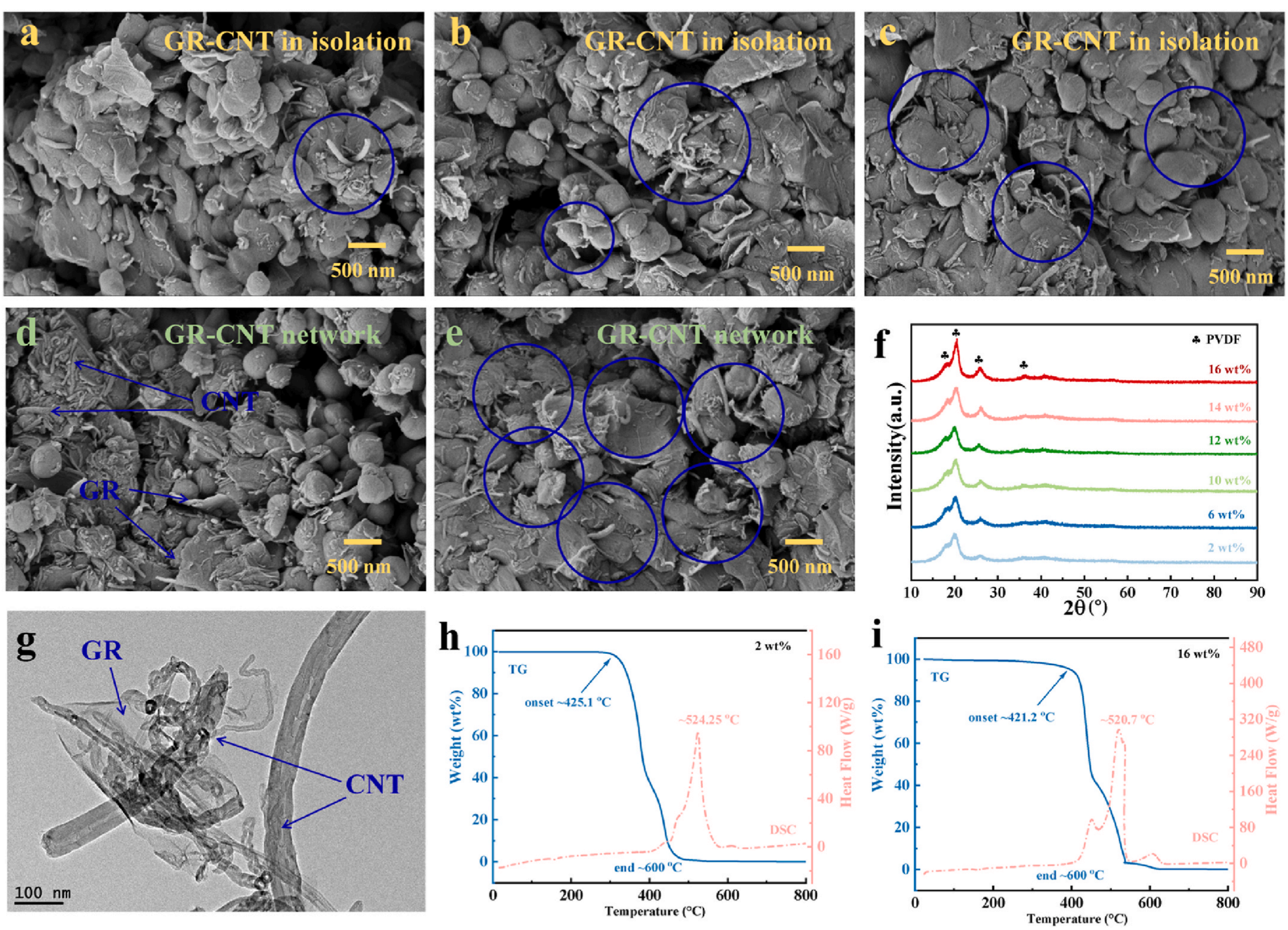

Fig. 1. FESEM images (a–e) and XRD patterns (f) of GR-CNT/PVDF composites with incremental GR-CNT content from 6 wt% to 16 wt% (a–e), respectively. TEM image (g) of GR-CNT powders. TG-DSC curves (h–i) of GR-CNT/PVDF composites.

2.2. Electrical conductivity

The microstructural changes from an isolated state to a 3D network via incremental GR-CNT incorporation in the PVDF matrix are portrayed in Fig. 1 and correlate with varying trends in electrical conductivity. For metacomposites containing 2–12 wt% GR-CNTs, the σ_{ac} demonstrated a consistent increase with the frequency. However, for those with 14 and 16 wt% GR-CNTs, σ_{ac} exhibited a decline as the frequency increased. Isolated GR-CNT clusters supported free carriers' movement through thermal activation, prompting them to travel to adjacent lattice points in a "jumping" manner, a process known as hopping conductivity. In Fig. 2a, the dashed lines represent fitting data according to Jonscher's power law [4–6]:

$$\sigma_{ac} = \sigma_{dc} + A(2\pi f)^n \tag{1}$$

Where σ_{dc} denotes the direct current (DC) conductivity, A is the pre-exponential factor, $2\pi f$ represents the angular frequency, and n is the fractional exponent. The congruence between the theoretical predictions and experimental observations exemplifies the characteristic frequency-dependence of σ_{ac}.

Conversely, with the establishment of 3D conductive carbon networks, a transition to metal-like conductivity was observed, along with a skin effect at high frequencies (Fig. 2b). The experimental data for metacomposites with high GR-CNT content aligned well with predictions from the Drude model [4–6]:

$$\sigma_{ac} = \frac{\sigma_{dc}\omega_\tau^2}{\omega^2 + \omega_\tau^2} \tag{2}$$

Where σ_{dc} is the DC conductivity, ω denotes the angular frequency of the applied electrical frequency, and ω_τ is the relaxation rate. Fig. 2c illustrates the variation of σ_{ac} with different GR-CNT contents at 100 MHz. Below 12 wt% GR-CNT, a gradual increase in σ_{ac} is apparent, indicative of a dispersed conductive phase. Between 12 wt% and 14 wt%, there is a marked increase, manifesting the percolation threshold's effects.

2.3. Low-dispersion ultraweakly ε'-negative response

As depicted in Fig. 3, the GR and CNTs served not only as microstructural components but also as contributors to free carriers in a plasma state. In samples with lower GR-CNT content, strengthened interfacial polarization under the external electric field induced hopping conduction. Increasing the conductive content, resulted in the GR-CNTs and PVDF forming a uniform 3D conductive network, facilitating metal-like electron transfer. Based on the Drude model (Equation (3)), a relation between ω_p (plasma frequency) and ω (electric field frequency) revealed the condition for negative ε' ($\omega < \omega_p$) [6–9].

$$\varepsilon' = 1 - \frac{\omega_p^2}{\omega^2 + \Gamma_D^2} \tag{3}$$

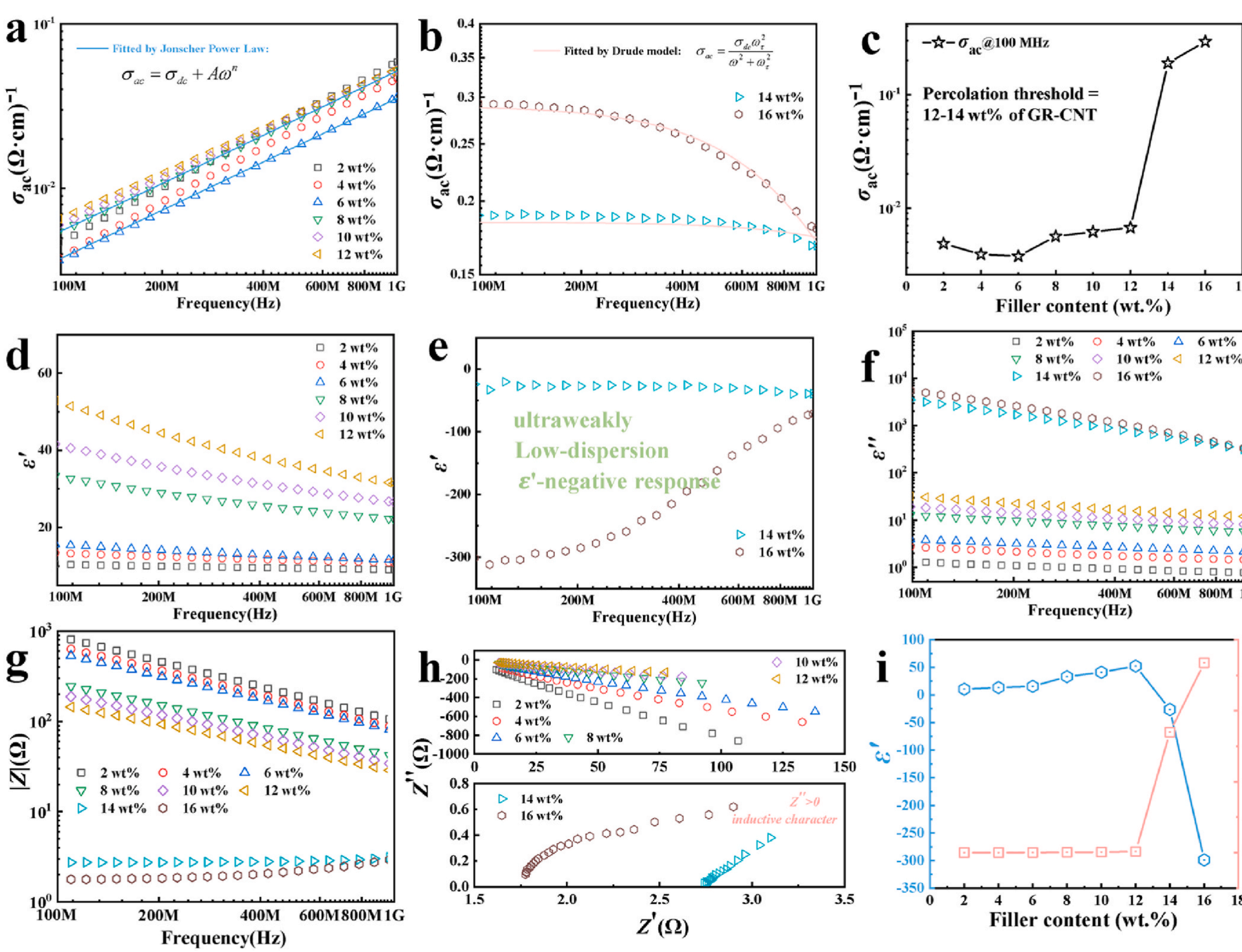

Fig. 2. Frequency dependences of AC conductivity (a–b), complex permittivity (d–f), impedance modulus (g), and Nyquist plots reactance (h) for GR-CNT/PVDF composites, with variances in σ_{ac} and ε' as a function of filler content depicted in (c, i).

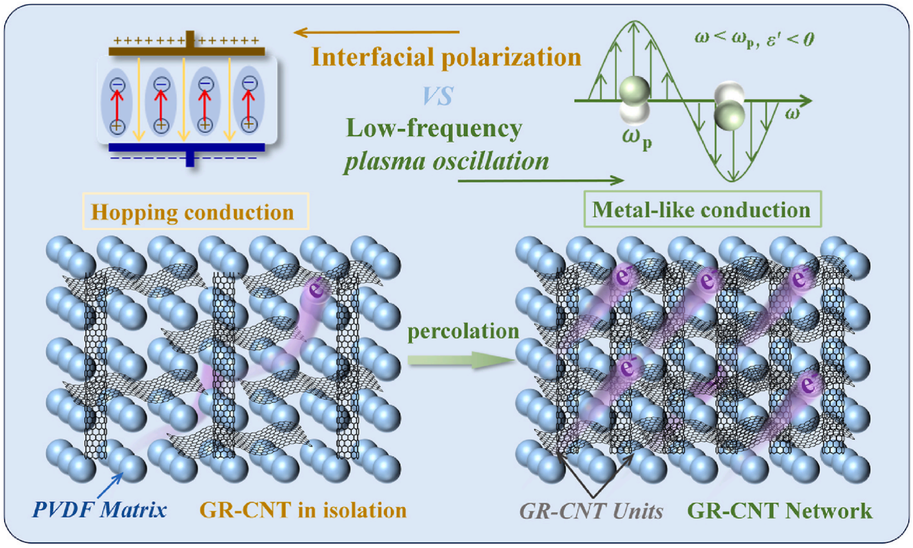

Fig. 3. Schematic for the generation mechanism of epsilon-negative response with microstructural evolution.

$$\omega_p = \sqrt{\frac{ne^2}{m\varepsilon_0}} \tag{4}$$

Here, ω_p is the plasma frequency that determines the ε'-response strength. It relates with the concentration of free carriers (n) in composites. The ω represents the electric field frequency, Γ_D is the damping constant, ε_0 is vacuum permittivity (8.85×10^{-12} F/m), m is electron mass.

The composites with 2–12 wt% GR-CNTs exhibited positive values of ε' (<60) across the frequency range (Fig. 2d), attributed to interfacial polarization between the GR-CNTs and PVDF which was essentially different from the ε'-response. These positive ε' values increased progressively with higher GR-CNT content, signifying an expanded interface area. The ultra-weakly ε' values ($0< |\varepsilon'| < 1000$) were maintained at relatively low dispersion, indicating a stable response across frequencies and suggesting an epsilon-near-zero (ENZ) potential. Interestingly, the 14 wt% GR-CNT metacomposite exhibited low dispersion ($\varepsilon' \sim -20$) and negative permittivity ($\varepsilon' < 0$) across the frequency spectrum, indicative of an ENZ phenomenon driven by plasma oscillations (Fig. 2e). The 16 wt% GR-CNTs metacomposite displayed ε' values commencing at −300 and gradually rising to −60 as the frequency reached 1 GHz.

Dielectric loss in the metacomposites was assessed by comparing the imaginary part of the permittivity (ε''), which normally includes relaxation loss (ε_r'') and conduction loss (ε_c''). The decreasing trend with frequency in various compositions indicated a dominant influence from conduction loss, while significantly heightened values ($>10^3$) in 14 and 16 wt% metacomposites unveiled the formation of 3D conductive networks (Fig. 2f). Fig. 2i simplified the complex permittivity properties at 100 MHz for varying filler contents, confirming the percolation threshold between 12 and 14 wt% due to structural enhancement by GR, CNT, and semiconductive PVDF.

2.4. Impedance character

Composites could function as capacitors, resistors, and inductors upon exposure to external alternating electric fields. The negative value of reactance (Z''), where $Z'' = Z_L - Z_C$ (with Z_L as inductive reactance and Z_C as capacitive reactance), explained the equivalent capacitive characteristics in composites. Conversely, a positive Z'' value suggested inductive properties. Fig. 2g and h displayed the Nyquist plots, illustrating the electrical behavior of the composite samples. For composites with GR-CNTs content from 2 to 12 wt%, the corresponding Z'' values were consistently negative. Conversely, for compositions with 14 and 16 wt% GR-CNTs, the Z'' values transitioned to positive, indicating an inductive circuit presence. The intrinsic correlation between impedance (ε') and reactance (Z'') in negative materials can be expressed as [6–9]:

$$\varepsilon' = -\frac{Z''}{\omega C_0\left(Z'^2 + Z''^2 \right)} \tag{5}$$

Here, C₀ represents the vacuum capacitance, and Z' indicates the resistance. A negative ε' correlates with a positive Z'', denoting an inductive circuit. For composites with 2–12 wt% content, |Z| diminished as the frequency increased from 100 MHz to 1 GHz, describable by Refs. [7–10]:

$$|Z| = \frac{1}{\sqrt{G^2 + \omega^2 C^2}} \tag{6}$$

Here, G and C represent the conductance and capacitance, respectively. A continuous increase in C for ε'-positive composites corresponded with the decreasing |Z|. However, this trend reversed for samples with 14 and 16 wt% content. A modest increase of |Z| with frequency in composites containing 14 wt% and 16 wt% GR-CNTs, in contrast to the behavior observed in samples with lower content, clearly signified a distinct electrical response, suggestive of an inductive effect. Furthermore, the modulus exhibited a decrease in magnitude as the GR-CNT content increased, which confirms the formation of a more conductive network.

2.5. EM simulation and shielding effectiveness

The incorporation of structural conductive design in ε'-negative materials may enhance the transformation of EM waves into conduction loss (ε_c'') and subsequent heat loss, representing a preferred choice for EM shielding [11,12]. CST via software was utilized to model the interactions between EM waves and shielding composites and to examine the propagation characteristics of EM waves. In Fig. 4a–d, the distribution of the electric field vector at 1 GHz for composites with varying GR-CNTs content and a thickness of 1 mm is depicted. An increase in GR-CNTs content markedly augmented the EM shielding, transitioning from a gradient dispersion (2–4 wt% GR-CNTs) to a robust blocking mode at 14 and 16 wt% GR-CNTs content metacomposites, due to the absorption of incident waves by an increasingly dense 3D conductive network, leading to greater conduction loss [13–17]. These simulation outcomes are in alignment with the anticipated low-frequency plasma

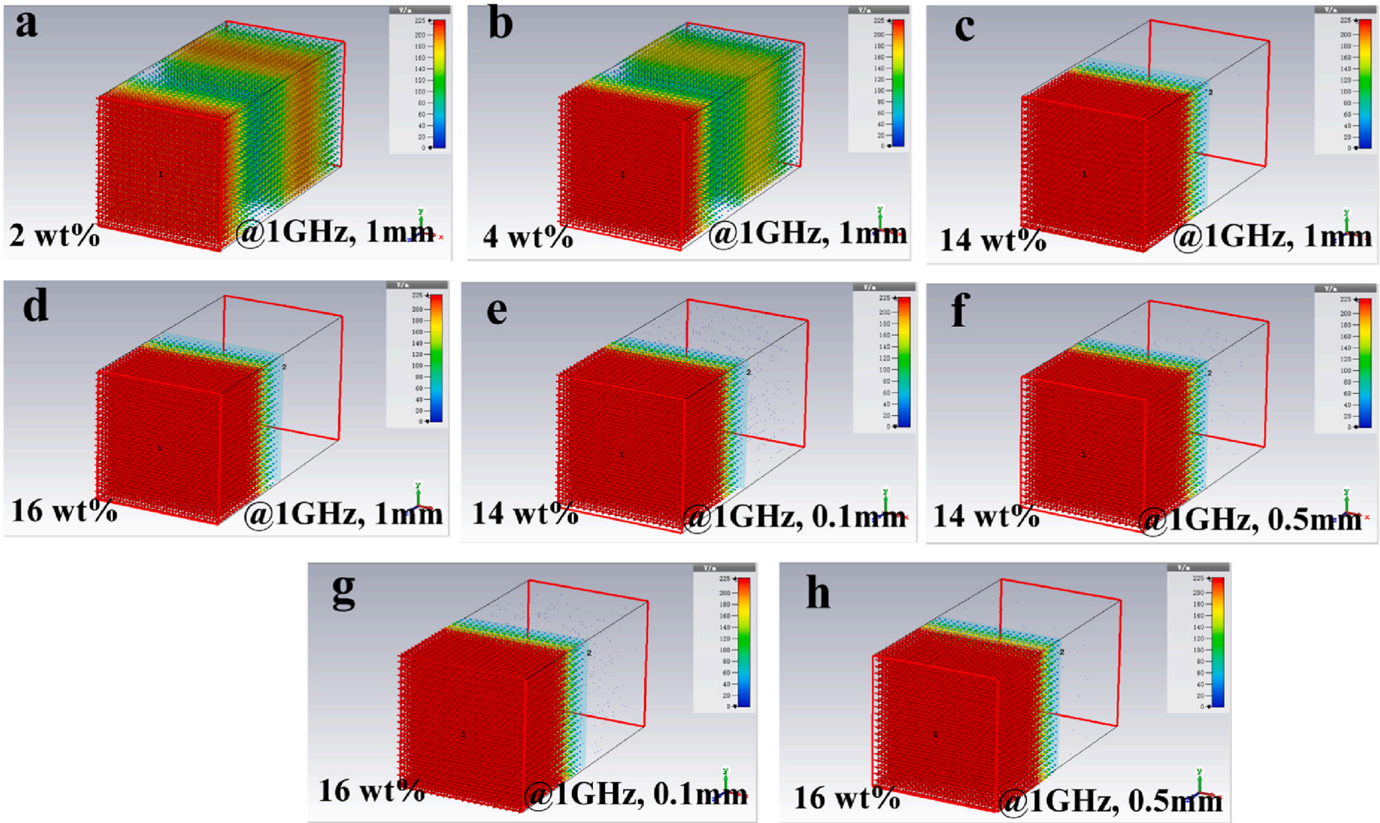

Fig. 4. The electric field vector distribution in GR-CNT/PVDF composites at 1 GHz (a–i), illustrates variations in GR-CNT content and composite thickness.

effects attributable to percolation and ENZ phenomena. Notably, reducing the sample thickness to 0.1 mm and 0.5 mm in 14–16 wt% GR-CNTs metacomposites did not diminish the EM shielding effect compared to the 1 mm samples (Fig. 4e–h). Such findings underscore the efficacy of 3D conductive networks and ENZ materials in enhancing EM shielding within the RF spectrum [18–26].

3. Conclusion

In this study, a 3D carbon network was synthesized within a PVDF matrix by dispersing GR-CNT building blocks randomly, resulting in a percolation effect that modified the electrical and dielectric attributes of the nanocomposites. The resulting metacomposites exhibited low-dispersion and ultraweak ε'-negative response ($\varepsilon' \sim -20$), reflective of the low-frequency plasmonic state of free carriers in the GR-CNT networks. The adjustable GR-CNT framework allowed precise control of the ε'-negative properties. CST software simulations confirmed the exciting EM shielding effect of materials with ε'-negative properties. The structural design approach of ternary metacomposites, which provides tunable ε'-negative responses in the RF range, opens new avenues for advancement in this field.

CRediT authorship contribution statement

Jiangnan Yuan: Writing – original draft, Visualization. **Yunlei Zhou:** Writing – review & editing. **Farid Manshaii:** Writing – review & editing. **Shaolei Wang:** Investigation, Data curation. **Junyi Yin:** Software. **Dongchan Li:** Supervision. **Shizhao Wang:** Visualization. **Yunpeng Qu:** Supervision, Funding acquisition.

Declaration of competing interest

The authors declare that they have no known competing financial interests or personal relationships that could have appeared to influence the work reported in this paper.

Data availability

Data will be made available on request.

Acknowledgments

This work was supported by the National Natural Science Foundation of China (Grant No. 52205593) and the Fund of Natural Science Special (Special Post) Research Foundation of Guizhou University (Grant No. 2023-032).

Appendix A. Supplementary data

Supplementary data to this article can be found online at https://doi.org/10.1016/j.coco.2024.101877.

References

[1] Z. Leng, Z. Yang, et al., Adv. Compos. Hybrid Mater. 6 (2023) 195.
[2] Y. Qu, Z. Wang, et al., Compos. Sci. Technol. 217 (2022) 109092.
[3] R. Ma, C. Cheng, et al., Ceram. Int. 47 (2021) 9971–9978.
[4] K. Sun, C. Wang, et al., Adv. Funct. Mater. (2023) 2306747.
[5] C. Deng, Y. Wu, et al., Compos. Commun. 43 (2023) 101724.
[6] Y. Zhou, Y. Qu, et al., Compos. Sci. Technol. 223 (2022) 109415.
[7] Y. Qu, P. Xie, et al., Ceram. Int. 49 (2023) 37407–37414.
[8] Z. Wang, K. Sun, et al., Acta Mater. 185 (2020) 412–419.
[9] Y. Qu, J. Wu, et al., Scripta Mater. 203 (2021) 114067.
[10] G. Fan, Z. Wang, et al., Scripta Mater. 190 (2021) 1–6.
[11] X. Tang, Z. Zhang, et al., Eng. Sci. 24 (2023) 920.
[12] Y. Qu, Q. Peng, et al., Compos. Commun. 44 (2023) 101750.
[13] P. Xie, Z. Shi, et al., Adv. Compos. Hybrid Mater. 5 (2022) 679–695.
[14] J. Tian, R. Fan, et al., J. Mater. Sci. Technol. 131 (2022) 91–99.
[15] Z. Zhang, M. Liu, et al., Adv. Compos. Hybrid Mater. 5 (2022) 1054–1066.
[16] Y. Qu, H. Wu, et al., Rare Met. 42 (2023) 4201–4211.

[17] Y. Wang, Z. Wei, et al., Appl. Phys. Lett. 123 (2023) 251701.
[18] M. Liu, H. Wu, et al., Adv. Compos. Hybrid Mater. 6 (2023) 217.
[19] H. Wu, Z. Zhang, et al., Adv. Compos. Hybrid Mater. 6 (2023) 206.
[20] Z. Zhang, M. Liu, et al., Adv. Compos. Hybrid Mater. 5 (2022) 1054–1066.
[21] P. Xie, Z. Shi, et al., Adv. Compos. Hybrid Mater. 5 (2022) 679–695.
[22] M. Liu, H. Wu, et al., Adv. Compos. Hybrid Mater. 5 (2022) 2021–2030.
[23] Y. Qu, Y. Zhou, et al., Rare Met. 43 (2024) 796–809.
[24] P. Xie, Y. Liu, et al., Adv. Compos. Hybrid Mater. 4 (2021) 173–185.
[25] H. Wu, Y. Zhong, et al., Adv. Compos. Hybrid Mater. 5 (2022) 419–430.
[26] Y. Hao, Z. Leng, et al., Carbon 212 (2023) 118156.